Topological Rainbow Concentrator Based on Synthetic Dimension

Cuicui Lu,[1,2,4,*] Chenyang Wang,[1] Meng Xiao,[3,†] Z. Q. Zhang,[2] and C. T. Chan[2,‡]

[1]Key Laboratory of Advanced Optoelectronic Quantum Architecture and Measurements of Ministry of Education, Beijing Key Laboratory of Nanophotonics and Ultrafine Optoelectronic Systems, School of Physics, Beijing Institute of Technology, Beijing 100081, China

[2]Department of Physics, The Hong Kong University of Science and Technology, Clear Water Bay, Kowloon, Hong Kong, China

[3]Key Laboratory of Artificial Micro- and Nano-Structures of Ministry of Education, School of Physics and Technology, Wuhan University, Wuhan 430072, China

[4]Collaborative Innovation Center of Light Manipulations and Applications, Shandong Normal University, Jinan 250358, China

(Received 22 September 2020; accepted 24 February 2021; published 19 March 2021)

Synthetic dimension provides a new platform for realizing topological photonic devices. Here, we propose a method to realize a rainbow concentrator of topological photonic states based on the synthetic dimension concept. The synthetic dimension is constructed using a translational degree of freedom of the nanostructures inside the unit cell of a two-dimensional photonic crystal. The translational deformation induces a nontrivial topology in the synthetic dimension, which gives rise to robust interface states at different frequencies. The topological rainbow can trap states with different frequencies, controlled by tuning the spatial modulation of interface state group velocities. The operation frequency as well as the bandwidth of the topological rainbow can be easily tuned by controlling the band gap of the photonic crystal. The topological principle can be applied to photonic crystals of any symmetry and arbitrary material composition, as long as a complete band gap exists. This Letter provides a new and general scheme for the realization of a topological rainbow concentrator and will be useful for the development of topological photonic devices.

DOI: 10.1103/PhysRevLett.126.113902

Rainbow trapping, which disperses and traps states with different frequency components at different spatial positions [1], is useful for applications that require temporary storages of light [2], enhanced light-matter interaction [3], and frequency routing [4,5]. However, the existing designs of rainbow trapping only realize the function of splitting the light signal to different positions without concentrating weak signals. Here, we introduce the concept of the rainbow concentrator, which can collect weak signals and map different frequency components to different spatial locations. Compared with traditional concentrators using plasmonic structures [4,6] or transformation optics [7–9], which either work in a narrow bandwidth or exhibit no frequency resolution or both, a rainbow concentrator works at multiple frequencies and hence greatly enhances the capability of a single photonic device. Moreover, there is intrinsic loss for plasmonic structures. As for transformation optics system, a slight deviation from the designed parameters usually severely compromises the functionality. It is desired to develop a novel method to construct rainbow concentrators.

In recent years, topological concepts offer a platform for discovering new physics and a new paradigm for designing next generation devices. Motivated by the advances made in condensed matter physics, there has been a recent surge in attempts to realize topological states in acoustic, mechanical, microwave, and optical systems [10–14]. In the realm of topological photonics, initial attention mainly focused on realizing unidirectional surface modes [15,16]. Various implementations successfully demonstrated the robustness of topological optical states against disorder, leading to new possibilities in designing photonic devices whose functionalities are topologically protected [17,18]. More recently, topological properties have also been studied in systems with additional degrees of freedom, supplementing the apparent geometrical dimensions. Such additional degrees of freedom, frequently referred to as "synthetic dimensions," expand the realm of topological photonics, as it breaks the constraint that the dimension of a physical system should be equal to or smaller than the geometrical dimension. It enables the investigation of higher-dimensional physics in two-dimensional photonic chips [19–21], simplifies the photonic structure [22], and brings new opportunities in manipulating the internal degrees of freedom of light [23,24].

Here, we realize a topological rainbow concentrator by constructing a synthetic dimension. Our system comprises an interface formed by a two-dimensional photonic crystal (PC) with a square lattice on one side and the same PC with translational deformations on the other. Our device can concentrate weak signals and distribute different frequency components of topological states to different locations

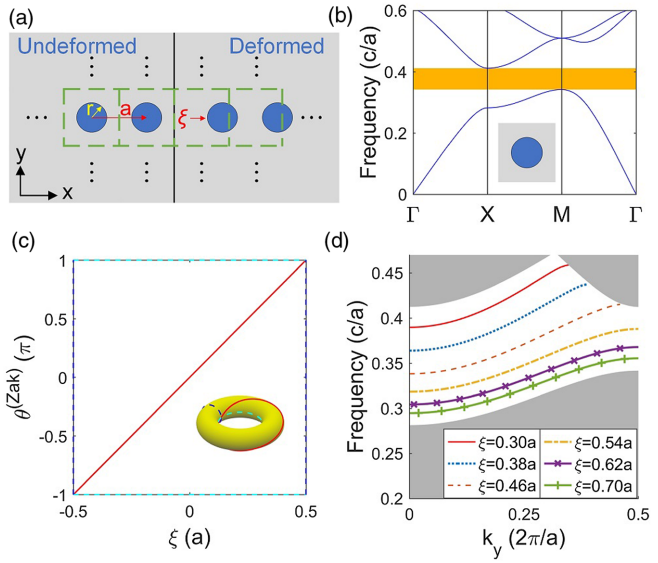

FIG. 1. (a) Schematic diagram of the structure with dielectric columns (blue) in a square lattice surrounded by air. (b) The dispersion bands of the TM mode bulk states with a complete band gap (orange stripe). (c) Zak phase evolution as a function of ξ. The torus is constructed by gluing the equivalent edges. (d) Dispersion bands of the TM interface states. The gray regions denote the projected bulk bands.

along the interface, enabling frequency routing in a real space. The topological principle that ensures the robustness of our device is interpreted by introducing a synthetic dimension. Moreover, this device only requires common dielectric optical material and can surpass the limit set by the intrinsic loss in plasmonic systems. The principle discussed here is free of material restriction and can be easily generalized to other wave systems, including but not limited to acoustics, elastic waves, and also cold atoms, which can demonstrate similar physics. Our Letter can bring new insight in designing photonic devices with topologically robust functionalities and facilitates applications such as photonic routers, photonic information processing, and light storage.

We first consider a typical dielectric PC comprising a square lattice of dielectric cylinders embedded in air. The eigenstates can be labeled by the Bloch wave vector (k_x, k_y), forming a 2D parametric space. We now define the position of the cylinders relative to the surface of the PC and introduce a displacement parameter ξ in the x direction [as defined in Fig. 1(a)]. This translational parameter ξ will be regarded as a synthetic dimension. The parameter ξ and the Bloch wave vectors (k_x, k_y) together form a 3D parametric space (k_x, k_y, ξ). Because the three parameters are all periodic, the periodic gauge can be imposed on eigenstates, which is $|\psi_n(k_x+2\pi/a, k_y, \xi)\rangle = |\psi_n(k_x, k_y+2\pi/a, \xi)\rangle = |\psi_n(k_x, k_y, \xi+a)\rangle = |\psi_n(k_x, k_y, \xi)\rangle$, where $|\psi_n(k_x, k_y, \xi)\rangle$ denotes the eigen Bloch state with parameter (k_x, k_y, ξ) and band number n. If we fix k_y, the two parameters (k_x, ξ) form a torus and the eigenstates of this 2D subsystem are topologically nontrivial. Here the topology is characterized by Chern numbers, which are the winding numbers of the one-dimensional Zak phase as ξ changes by one lattice constant. For each ξ, the Zak phase of the nth band $\theta_n^{(\mathrm{Zak})}(k_y, \xi)$ is defined as [25]

$$\theta_n^{(\mathrm{Zak})}(k_y, \xi) = \int_{-\frac{\pi}{a}}^{\frac{\pi}{a}} \langle u_n(k_x, k_y, \xi) \left| i \frac{\partial}{\partial k_x} \right| u_n(k_x, k_y, \xi) \rangle dk_x, \tag{1}$$

where $|u_n(k_x, k_y, \xi)\rangle = e^{-ik\cdot\hat{r}}|\psi_n(k_x, k_y, \xi)\rangle$ is the periodic part of the Bloch state of the nth band with parameter (k_x, k_y, ξ). When k_y is fixed and ξ varies from $-a/2$ to $a/2$, the winding of Zak phase divided by 2π gives the Chern number of this band [26], as is expressed in Eq. (2),

$$C_n(k_y) = \frac{1}{2\pi} \int_{-a/2}^{a/2} \partial_\xi \theta_n^{(\mathrm{Zak})}(k_y, \xi) d\xi. \tag{2}$$

For a fixed k_y, the 2D PC is effectively reduced to a 1D system. In 1D PCs, the Zak phase is equivalent to the Wannier center by the relation $\theta_n^{(\mathrm{Zak})} = 2\pi/a \int_{-\infty}^{\infty} x|W_n(x)|^2 dx$, where $W_n(x)$ denotes the Wannier function of the nth band [25,27]. The Zak phase of the 2D PC with a fixed k_y can be regarded as the center of a "quasi-one-dimensional" Wannier function, which is defined as a partial Fourier transformation of the Bloch functions in the x direction, as is shown in Supplemental Material, Sec. I [28]. When ξ changes from 0 to a, the center of the quasi-one-dimensional Wannier function will also change by a lattice constant, so that the Zak phase changes with the lattice translational deformation as indicated in Eq. (3). We note here that synthetic dimension has been introduced previously (see, in particular, Ref. [32]), however, a rainbow concentrator cannot be realized with the system discussed in Ref. [32], wherein each sample only exhibits one isolated surface state,

$$\theta_n^{(\mathrm{Zak})}(k_y, \xi) = \theta_n^{(\mathrm{Zak})}(k_y, 0) + \frac{2\pi}{a}\xi (\mathrm{mod}\ 2\pi). \tag{3}$$

For a fixed k_y, as we gradually increase ξ by a, Eq. (3) indicates that $\theta_n^{(\mathrm{Zak})}(k_y, \xi)$ increases by 2π. We then see that the Chern number of each isolated band is equal to 1. In a more general setting, which involves multiple bands, the total Chern number characterizing a gap is equal to the sum of the Chern number of the bands below that gap, which also provides a method to construct an artificial system with a desired value of Chern numbers. This topological characteristic is constructed by a translational degree of freedom of the microstructure within the unit cell and, as such, it exhibits little restriction on the material and the space group symmetry. In the Supplemental Material [28], we show that the same principle can be applied to other lattices.

The nontrivial topology in the subspace (k_x, ξ) naturally leads to interface states by joining the undeformed structure and the deformed structure together, as illustrated in Fig. 1(a). The square unit cell contains a dielectric cylinder, which has a refractive index $n = 2.4$ (common dielectric materials have refractive indices ranging from 1.3 to 3.5 in optical frequencies), and the radius is $r = 0.2715a$, where a is the lattice constant. The bulk dispersion of the transverse magnetic (TM) modes are shown in Fig. 1(b). While we focus on the TM modes, the transverse electric modes can be studied in a similar way. As shown in Fig. 1(b), there is an absolute band gap from $0.34\,c/a$ to $0.41\,c/a$. The band gap can be enlarged by increasing the dielectric constant or optimizing the radius of the cylinder. We numerically calculate the Zak phase evolution of the first bulk band by using the Wilson loop approach when changes by one lattice constant [33]. As shown in Fig. 1(c), when ξ changes by a period, the Zak phase changes by 2π. This conclusion holds for all fixed k_y (the component of wave vector in the y direction) and is consistent with Eq. (3). Because of the nontrivial topology in the subspace (k_x, ξ), i.e., each isolated band with a fixed k_y possesses a Chern number 1, a series of ξ-dependent interface states can be constructed when ξ changes from 0 to a. For each k_y, there is always a range of ξ in which one interface state can be found in the gap, which is ensured by the bulk-edge correspondence [34,35]. The band dispersions of interface states as a function of k_y are shown in Fig. 1(d). Analogous to the topological pumping [34], the frequencies of dispersion bands of interface states decrease from the second bulk band to the first bulk band when ξ changes by one lattice constant.

After obtaining the dispersion of the interface states, we can study how the translational degree of freedom within the unit cell controls the regions of existence and the group velocities of the interface states. In Fig. 2(a), the group velocities of the interface states are plotted as a function of frequency and the synthetic dimension. Here, we consider the frequency range of the complete band gap region for rainbow design, where the light can only propagate along the interface. The left and right dark regions in Fig. 2(a) represent the regions where no interface states exist, and in the middle bright region, the interface states exist. The color in the middle bright region indicates the group velocity of the interface states. The two cyan dashed lines mark the boundaries of the three regions, which correspond to the minima or maxima of the dispersion bands of a certain ξ. As is shown in Fig. 1(d), the minima and maxima of dispersion bands correspond to states with $k_y = 0$ and $k_y = \pi/a$, respectively. The four critical points ξ_{c1}, ξ_{c2}, ξ_{c3}, and ξ_{c4} are the intersectional points of the boundaries of the regions and the edge of band gap, which partition the synthetic dimension into five intervals. In the interval $[0, \xi_{c1}]$ or $[\xi_{c4}, a]$, interface states cannot exist; in the interval $[\xi_{c2}, \xi_{c3}]$, interface states with all frequencies

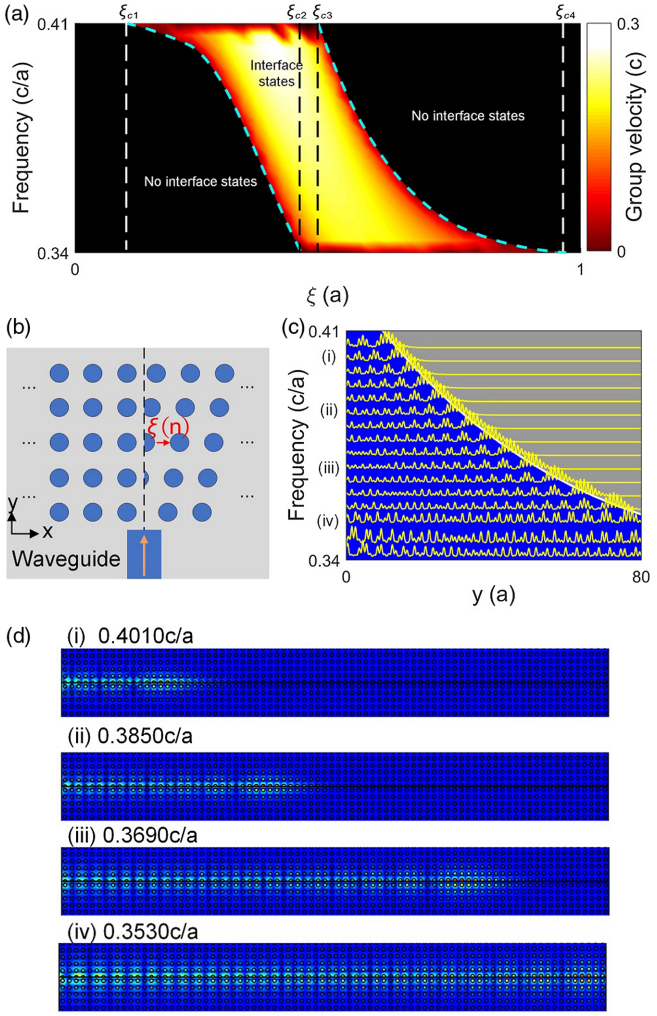

FIG. 2. (a) The group velocity distribution shown in the dispersion diagram of synthetic space. The cyan dotted lines denote the boundaries between the regions where interface states exist and do not exist. (b) The schematic diagram of topological rainbow concentrator, with light coupled in using a dielectric waveguide. (c) Normalized energy density distributions along the interface. The blue and gray parts are regions of existence and nonexistence of interface states. (d) Electric intensity distributions of the interface states corresponding to the frequencies marked in roman numbers in (c).

over the complete band gap can exist; and in the interval $[\xi_{c1}, \xi_{c2}]$ and $[\xi_{c3}, \xi_{c4}]$, only the interface states with a certain frequency range can exist, and the frequency range will change when ξ changes.

Now, instead of a fixed k_y, which requires a well-defined periodicity along the y direction in 2D PCs, we modulate ξ in the y direction as shown in Fig. 2(b). The parameter ξ of the nth row (in the y direction) is denoted as $\xi(n)$. The simplest way is the linear modulation of ξ,

$$\xi(n) = (\xi_N - \xi_1)(n-1)/(N-1) + \xi_1, \qquad (4)$$

where ξ_1 and ξ_N are the translational parameters of the first and last layers. Other constructions for modulation of $\xi(n)$

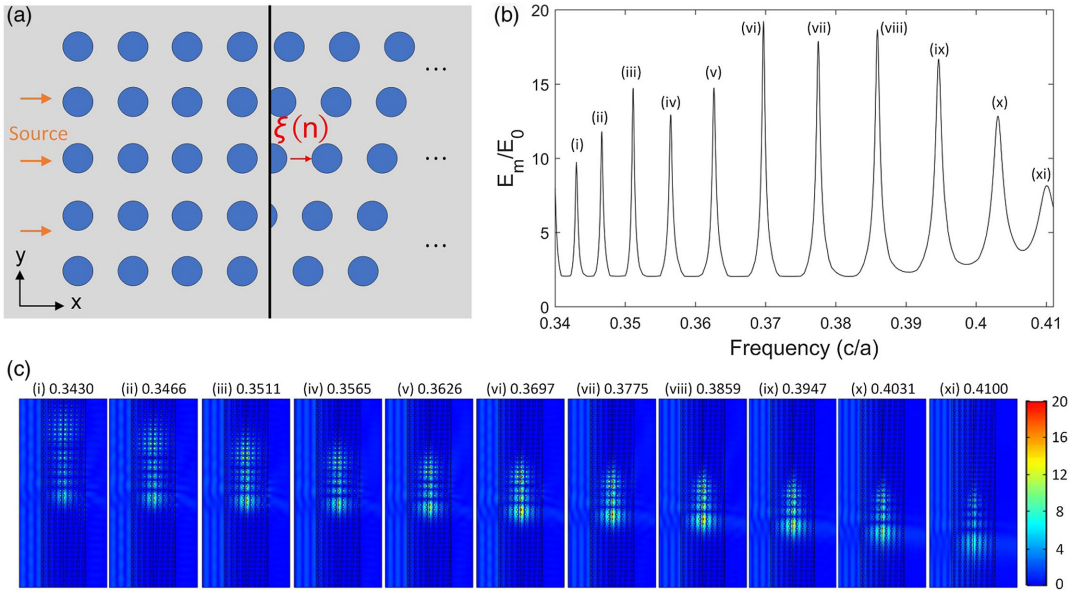

FIG. 3. (a) The schematic diagram of the structure excited by plane wave along the x direction. (b) The spectrum of enhancement rate of the maximal intensity over the incident plane wave E_m/E_0. (c) The electric intensity distribution of the peaks in (b), normalized by the intensity of incident plane wave E_0.

are also feasible; for example, the sinusoidal modulation of ξ is discussed in detail in Fig. S2 in the Supplemental Material [28]. The spatial modulation of the $\xi(n)$ will shift each row of the lattice laterally, while the row shifting will deform the square lattice of the right-hand side PC, and the band gap becomes wider with the introduction of synthetic dimension (see Fig. S3 in the Supplemental Material [28] for the dispersion bands of the deformed structure). If the spatial change of ξ is smooth and mild enough, the structure is locally equivalent to that with homogeneous displacement as in Fig. 1(a). From Fig. 2(a), we see that, for each frequency, there are two extreme values of ξ at which the system no longer supports any interface state. Combined with Eq. (4), we can obtain the y coordinate where the local effect ξ no longer supports any interface state. This relation is shown in Fig. 2(c) with the white curve dividing the phase space into two regions: blue with interface states and gray without interface states. If the parameters ξ_1, ξ_N satisfy $\xi_{c2} < \xi_1 < \xi_{c3} < \xi_N$, light with frequency inside the band gap can be coupled into the structure and will propagate along the interface, until it reaches the position where the interface states are no longer supported locally. In our calculation, the light is coupled in through a dielectric waveguide with the same material of the dielectric column and a width equal to the lattice constant. The critical points are $\xi_{c1} = 0.10a$, $\xi_{c2} = 0.45a$, $\xi_{c3} = 0.48a$, $\xi_{c4} = 0.97a$, and the parameters of the first and last layers are $\xi_1 = 0.45a$ and $\xi_N = 0.7a$. In Fig. 2(c), we show the normalized energy density distributions along the interface. The result shows that the lights of different frequencies stop at different positions, as predicted by the blue and gray regions. The electric intensity distributions around the interface are shown in Fig. 2(d), where the roman numbers correspond to the frequencies marked in Fig. 2(c).

Figure 2(c) shows that there is a maximum value of ξ at which the surface wave with a given frequency will stop propagating. Similarly, there is a minimum value of ξ above which the surface wave starts propagating. Hence, if we construct an interface with a linear modulation of $\xi(n)$ with parameters ξ_1, ξ_N and the modulation satisfying $\xi_1 < \xi_{c1}$, $\xi_N > \xi_{c4}$, light waves of all frequencies are trapped in the region where the interface states exist. Since the maximum and minimum values of ξ also depend on the frequency [see Fig. 2(a)], the position where an interface state is concentrated is a function of frequency; i.e., we have thus realized a topological rainbow concentrator.

The topological rainbow concentrator can be excited from the left-hand side of the sample as shown in Fig. 3(a) by a plane wave source. Here, each side consists of four lattices away from the surface. Figure 3(b) shows the spectrum of enhancement ratio of the maximal electric intensity of the rainbow (denoted by E_m) over the electric intensity of the incident plane wave source (denoted by E_0). The peaks correspond to the localized eigenstates of the system, the electric intensity of which is shown in Fig. 3(c). Figure 3(c) shows the regions of the eigenstates are different for different frequencies. Meanwhile, the overlaps between modes can be greatly reduced by engineering the lattice (see Supplemental Material, Secs. IV and V) [28]. Moreover, the number of peaks is controlled by N in Eq. (4); the larger N is, the more peaks we have, and the enhancement ratio can be greatly enhanced by increasing the number of lattices on each side of the surface. As the

topology of (k_x, ξ) space has no restriction on the geometric symmetry and materials, the discussion above is also applicable to different lattice types and different materials, as long as the dispersion band of the bulk photonic crystal has a complete band gap. In addition, the frequencies of some conventional defect modes can be tuned by changing some parameters, and some of them are highly customizable. Most of these highly customizable modes can be converted into topological ones with proper design by adopting our method through constructing a synthetic dimension with translation from zero to one lattice constant. In the Supplemental Material, Secs. IV and V [28], the topological rainbow concentrators constructed by triangular lattice and honeycomb lattice are discussed, and the design and modulation of the operation frequency range are discussed in the Supplemental Material, Sec. VI [28]. Moreover, topological pumping is robust against disorder [36] and random scaling of geometry (see Supplemental Material [28], Sec. VII for more details).

In conclusion, we proposed a topological rainbow concentrator using the translational degree of freedom of the inclusions inside the unit cell of 2D PCs. The synthetic dimension induces nontrivial topology in the 2D subspace (k_x, ξ), analogous to topological pumping. The nontrivial topology determines the existence of interface states at the boundary. The properties of topological rainbow can be controlled by tuning the group velocities of interface states. The rainbow structures are immune to disorder in the bulk and can break the usual restrictions of narrow operation bandwidth or single operational frequency, which are typical limiting factors of previous fixed photonic lattices. The operation principle does not depend on lattice symmetry or material properties, and so the synthetic dimension idea can be applied to just about any type of PCs. The topological rainbow concentrator can be realized in near infrared and visible light regions and provides a new platform for the realization of topological photonic devices.

This work was supported by the National Natural Science Foundation of China under Grants No. 91850117, No. 11654003, No. 11604378, and No. 11904264; by Beijing Institute of Technology Research Fund Program for Young Scholars; and by Hong Kong Research Grants Council through Grant No. 16307420.

*Corresponding author.
cuicuilu@bit.edu.cn
†Corresponding author.
phmxiao@whu.edu.cn
‡Corresponding author.
phchan@ust.hk

[1] K. L. Tsakmakidis, A. D. Boardman, and O. Hess, Nature (London) **450**, 397 (2007).
[2] M. F. Yanik and S. Fan, Phys. Rev. Lett. **92**, 083901 (2004).
[3] M. Notomi, K. Yamada, A. Shinya, J. Takahashi, C. Takahashi, and I. Yokohama, Phys. Rev. Lett. **87**, 253902 (2001).
[4] Q. Gan, Y. J. Ding, and F. J. Bartoli, Phys. Rev. Lett. **102**, 056801 (2009).
[5] J. B. Khurgin, Adv. Opt. Photonics **2**, 287 (2010).
[6] J. A. Schuller, E. S. Barnard, W. Cai, Y. C. Jun, J. S. White, and M. L. Brongersma, Nat. Mater. **9**, 193 (2010).
[7] M. Rahm, D. Schurig, D. A. Roberts, S. A. Cummer, D. R. Smith, and J. B. Pendry, Photonics Nanostruct. Fundam. Appl. **6**, 87 (2008).
[8] C. Navau, J. Prat-Camps, and A. Sanchez, Phys. Rev. Lett. **109**, 263903 (2012).
[9] C. Li, L. Xu, L. Zhu, S. Zou, Q. H. Liu, Z. Wang, and H. Chen, Phys. Rev. Lett. **121**, 104501 (2018).
[10] Z. Wang, Y. Chong, J. D. Joannopoulos, and M. Soljačić, Nature (London) **461**, 772 (2009).
[11] J. Lu, C. Qiu, M. Ke, and Z. Liu, Phys. Rev. Lett. **116**, 093901 (2016).
[12] R. Süsstrunk and S. D. Huber, Proc. Natl. Acad. Sci. U.S.A. **113**, E4767 (2016).
[13] M. Hafezi, S. Mittal, J. Fan, A. Migdall, and J. M. Taylor, Nat. Photonics **7**, 1001 (2013).
[14] Z. Tian, C. Shen, J. Li, E. Reit, H. Bachman, J. E. S. Socolar, S. A. Cummer, and T. J. Huang, Nat. Commun. **11**, 762 (2020).
[15] J. Dong, X. Chen, H. Zhu, Y. Wang, and X. Zhang, Nat. Mater. **16**, 298 (2017).
[16] A. B. Khanikaev, S. Hossein Mousavi, W. Tse, M. Kargarian, A. H. MacDonald, and G. Shvets, Nat. Mater. **12**, 233 (2013).
[17] B. Zhen, C. W. Hsu, L. Lu, A. D. Stone, and M. Soljačić, Phys. Rev. Lett. **113**, 257401 (2014).
[18] Y. Guo, M. Xiao, and S. Fan, Phys. Rev. Lett. **119**, 167401 (2017).
[19] O. Zilberberg, S. Huang, J. Guglielmon, M. Wang, K. P. Chen, Y. E. Kraus, and M. C. Rechtsman, Nature (London) **553**, 59 (2018).
[20] L. Yuan, Q. Lin, M. Xiao, and S. Fan, Optica **5**, 1396 (2018).
[21] T. Ozawa and H. M. Price, Nat. Rev. Phys. **1**, 349 (2019).
[22] A. Dutt, Q. Lin, L. Yuan, M. Minkov, M. Xiao, and S. Fan, Science **367**, 59 (2020).
[23] X. F. Zhou, X. W. Luo, S. Wang, G. C. Guo, X. Zhou, H. Pu, and Z. W. Zhou, Phys. Rev. Lett. **118**, 083603 (2017).
[24] X. W. Luo, X. Zhou, J. S. Xu, C. F. Li, G. C. Guo, C. Zhang, and Z. W. Zhou, Nat. Commun. **8**, 16097 (2017).
[25] J. Zak, Phys. Rev. Lett. **62**, 2747 (1989).
[26] H. Weng, R. Yu, X. Hu, X. Dai, and Z. Fang, Adv. Phys. **64**, 227 (2015).
[27] N. Marzari, A. A. Mostofi, J. R. Yates, I. Souza, and D. Vanderbilt, Rev. Mod. Phys. **84**, 1419 (2012).
[28] See Supplemental Material at http://link.aps.org/supplemental/10.1103/PhysRevLett.126.113902 for Wannier functions, sinusoidal modulation of the synthetic dimension, dispersion bands of the deformed structure with different translational deformations, rainbow concentrator of triangle lattice structures, rainbow concentrator of honeycomb lattice

structures, design and control of operation bandwidth, and rainbow concentrator with disorders, which includes Refs. [29–31].

[29] N. Marzari and D. Vanderbilt, Phys. Rev. B **56**, 12847 (1997).

[30] S. Raghu and F. D. M. Haldane, Phys. Rev. A **78**, 033834 (2008).

[31] Y. Zhang *et al.*, Nat. Commun. **10**, 4279 (2019).

[32] Y. Nakata, Y. Ito, Y. Nakamura, and R. Shindou, Phys. Rev. Lett. **124**, 073901 (2020).

[33] W. Benalcazar, B. Bernevig, and T. Hughes, Science **357**, 61 (2017).

[34] D. J. Thouless, Phys. Rev. B **27**, 6083 (1983).

[35] D. Vanderbilt, *Berry Phases in Electronic Structure Theory: Electric Polarization, Orbital Magnetization and Topological Insulators* (Cambridge University Press, Cambridge, England, 2018).

[36] D. Xiao, M. C. Chang, and Q. Niu, Rev. Mod. Phys. **82**, 1959 (2010).